CHAPTER 2

Polysomnography in humans and animal models: basic procedures and analysis

Pablo Torterolo[1,2], Joaquín Gonzalez[1], Santiago Castro-Zaballa[1], Matías Cavelli[1,3], Alejandra Mondino[1,4], Claudia Pascovich[1,5], Nicolás Rubido[6,7], Eric Murillo-Rodríguez[2,8] and Giancarlo Vanini[4]

[1]Laboratorio de Neurobiología del Sueño, Departamento de Fisiología, Facultad de Medicina, Universidad de la República, Montevideo, Uruguay; [2]Intercontinental Neuroscience Research Group, Mérida, Yucatán, México; [3]Department of Psychiatry, University of Wisconsin, Madison, WI, United States; [4]Department of Anesthesiology, University of Michigan, Ann Arbor, MI, United States; [5]Consciousness and Cognition Laboratory, Department of Psychology, University of Cambridge, Cambridge, United Kingdom; [6]Aberdeen Biomedical Imaging Centre, University of Aberdeen, Aberdeen, United Kingdom; [7]Instituto de Física, Facultad de Ciencias, Universidad de la República, Montevideo, Uruguay; [8]Laboratorio de Neurociencias Moleculares e Integrativas, Escuela de Medicina, División Ciencias de la Salud, Universidad Anáhuac Mayab, Mérida, Yucatán, Mexico

Introduction

Sleep is a critical physiological process. In most mammals and birds, two sleep states can be readily distinguished: rapid eye movement (REM) sleep and nonrapid eye movement (NREM) sleep [also called slow wave sleep (SWS)]. Together with the state of wakefulness (W), they constitute the wake-sleep cycle, one of the most visible circadian rhythms of the organism. Polysomnography (PSG) is the basic tool used to differentiate these behavioral states, both in clinical and human research settings, as well as in animal models.

Polysomnography

PSG is considered the gold standard method for studying sleep pathologies, and an essential tool for sleep research in both humans and animal models (Carskadon and Dement, 2017). It consists in the simultaneous recording of three biological signals: electroencephalogram (EEG), electromyogram (EMG), and eye movements [electrooculogram (EOG)]. Other bioelectrical signals can be also recorded according to the aim of the study (Keenan and Hirshkowitz, 2017).

Methodological Approaches for Sleep and Vigilance Research
ISBN 978-0-323-85235-7
https://doi.org/10.1016/B978-0-323-85235-7.00010-7

The EEG is produced by the summed electrical activities of populations of neurons, with a modest contribution from glial cells (Lopes da Silva, 2010). Pyramidal neurons of the cortex are the main contributors of the EEG signal, since they are arranged in palisades with the apical dendrites aligned perpendicularly to the cortical surface. The electrical fields generated by these neurons can be recorded by means of electrodes located from the cortical surface which is called electrocorticogram (ECoG) or intracranial EEG, or from the scalp (standard EEG). In the standard EEG, there is more distance between the source and the electrodes, and the signal is filtered out by the skull and scalp, which determines worse spatial resolution and reduction of the amplitude of the signal, mainly for oscillations higher than 30 Hz. On the contrary, oscillations up to 200 Hz can be easily recorded with the ECoG.

Several rhythmic oscillations can be observed in the EEG. These rhythms are generated in the thalamus and/or at cortical levels, and are modified according to the behavioral state (Torterolo et al., 2019). The EMG also changes abruptly across behavioral states, while the EOG tracks the eyes movements that characterize REM sleep.

Polysomnography in humans

Procedures

In standard EEG, the recording is obtained by placing electrodes on the scalp through a conductive gel. Individual electrodes or caps/nets with embedded electrodes are connected to a differential amplifier (Keenan and Hirshkowitz, 2017). Electrode locations and names are specified by the International 10–20 system for standard EEG clinical applications. However, a smaller number of electrodes may be used in PSG examination, which is incomplete for diagnosis of a neurological condition. Also, a smaller number of electrodes are typically used when recording term or premature neonates (Grigg-Damberger, 2016), which need to adapt the 10–20 system according to the neonate's head circumference. The number of electrodes may vary in research settings according to the goal of the study (up to 256 electrodes in high-density arrays).

The amplifiers increase (typically 1000–100,000 times or 60–100 dB of voltage gain) the voltage differences (ΔV) between the active and the referential electrode (or between two active electrodes in bipolar arrangements). The amplitude of the adult human standard EEG signal is about 10–100 μV.

Analog-to-digital sampling typically occurs at 256–512 Hz and 12 bits in clinical settings, but larger sampling rates are often used for research. Digital EEG signal is stored and can be filtered for display (and/or can be filtered before acquisition). Typical settings for the high-pass filter and a low-pass filter are 0.5–1 and 35–70 Hz, respectively. An additional notch (50 or 60 Hz) filter may be used to remove artifacts caused by electrical power lines.

For some conditions (usually for an evaluation for epilepsy surgery), the electrodes are placed on the brain surface by craniotomy to record the ECoG. In some cases, electrodes may be placed into deep brain structures such as the hippocampus. The procedure is the same as the standard EEG, but is typically recorded at higher sampling rates to observe the high-frequency components of the signals.

Since the EEG signal represents a ΔV between two electrodes, the EEG recording may be set in several ways or channels. This representation is known as montages. The montage could be bipolar, namely ΔV between two active electrodes; or referential, an active against a referential electrode. The reference could vary according to the objective of the study, but the referential electrode is usually placed in the midline position, both earlobes or mastoids. Also, an average of all the electrodes, Laplacian (Gordon and Rzempoluck, 2004) or computational such as reference electrode standardization technique or REST (Zheng et al., 2018), can be used as reference. For ECoG, it is also common to use the white matter as reference (Lachaux et al., 2003).

The EMG is recorded by bipolar electrodes on the skin above the muscle. The submental muscle is usually used, and the tibialis anterior can also be employed to record leg movements. The EOG is used to detect changes in eye movements, since moving the eyes creates changes in electrical potential (the eye behaves as a dipole). The surface electrodes are placed on the outer edge of each eye.

Other bioelectrical signals are often recorded. The respiratory effort is usually recorded by abdominal and thoracic piezoelectric bands that generate voltage changes with breathing movements. The ventilation can be also evaluated with respiratory inductance plethysmography by means of belts that capture the movement of chest and abdominal walls. The airflow measurement is carried out with a nasobuccal thermistor that detects temperature differences induced by breathing, and/or by a pressure transducer sensitive to air flow. In addition, signals such as oxygen saturation (by pulse oximetry), capnography (CO_2 sensor), electrocardiogram, snoring

sensor, moving sensor are frequently recorded. Finally, a video-recording synchronized with the PSG is commonly used to track the behavior during sleep.

Simplified portable PSG equipment can also be used to perform the recordings at home, either for clinical exploration or research. Wireless systems technologies have been also developed (Markwald et al., 2016).

Sleep characteristics in humans

The EEG recording of W is marked by the presence of high frequency and low-voltage oscillations (cortical activation) (Carskadon and Dement, 2017). During relaxed W with eyes closed, a high-amplitude alpha (8–12 Hz) oscillation appears mainly in the occipital (visual) cortex.

At sleep onset, adults enter into NREM sleep. In humans, three NREM sleep phases are recognized: N1, N2, and N3, according to the depth of the state. N1 represents the transition from W to sleep and is characterized by the presence of relatively low-voltage, mixed frequency waves with a prominence of activity in the theta (4–7 Hz) range. N1 is a shallow sleep stage with low-arousal threshold. N2 is an unequivocal stage of sleep that is characterized by the presence of two types of EEG events: sleep spindles and K-complexes. The former is an event with a spindle shape of 0.5–2 s in duration and a frequency of 12–14 Hz that contrast with the lower frequency of the EEG background activity. K-complexes are often associated with sleep spindles, and consist of a brief negative sharp high-voltage peak (usually greater than 100 μV), followed by a slower positive complex and a final negative peak. The presence of low frequency (0.5–4 Hz, delta oscillations) of high-amplitude waves characterizes the EEG during N3. REM sleep (also called stage R) is a deep sleep stage even though the EEG has low-voltage mixed frequency activity that is similar to W or N1; hence, it is also called "paradoxical" sleep. Saw-tooth waves (theta activity, 4–7 Hz) are often observed in conjunction with bursts of REMs in the EOG. A decrease in the activity of the EMG caused by muscle atonia also characterizes REM sleep; usually small muscles twitches are also identified in the EMG. REM sleep occurs approximately 90 min after the onset of sleep, a parameter known as REM sleep latency (Carskadon and Dement, 2011). Dreams occur mainly during this sleep state.

Nighttime sleep in humans is characterized by the presence of four to five sleep cycles. They comprise the period between the onset of sleep until the end of the first episode of REM sleep or the period from the end of a REM sleep episode to the end of the subsequent episode. The average duration of sleep cycles is approximately 90 min in adults. Young adults

spend 20%–28% of a night's sleep in REM sleep, 4%–5% in stage N1 sleep, 46%–50% in stage N2 sleep, and 20%–24% in stage N3. A shortening of sleep duration, which occurs in association with advancing age, is mainly related to the reduction in N3 sleep and REM sleep.

In newborns, W, immature NREM sleep known as quiet sleep (QS), immature REM sleep called active sleep (AS), and transitional or intermediate sleep (IS) are distinguished (Graven, 2006; Andre et al., 2010). The time spent in each stage of sleep differs throughout development. In the neonate, there is a predominance of AS. QS increases with gestational age and IS begins to disappear near term. The sleep-wake cycle in the neonatal stage also presents short sleep cycles (ultradian rhythm) (Mirmiran et al., 2003).

The results of the PSG are usually displayed in a hypnogram (see Fig. 2.1 for an example in animals). Thereafter, several parameters such as time, duration, and latencies of the different sleep phases are quantified.

Polysomnography in animal models

Procedures

Adapted PSG have been used to record different species. Rats, mice, and cats are the most utilized animal models for sleep research. Under general anesthesia, these animals are implanted with electrodes for PSG, usually, by means of stereotaxic surgery. Noninvasive PSG has been tried in dogs and equines, and is an option for veterinary medicine (Kis et al., 2014; Wohr et al., 2016; Gergely et al., 2020).

As the rat is one of the most common animal models employed to study sleep, we next describe the standard procedures to record and analyze the PSG in this model. In our experience, rats (Wistar, 250–300 g) are anesthetized by a mixture of ketamine-xylazine (90 mg/kg, 5 mg/kg i/p., respectively). The animals are positioned in a stereotaxic frame, and the skull is exposed. The brain electrical activity is recorded by means of stainless-steel screw electrodes (1.0 mm of diameter) placed on the skull with their tips touching the dura mater, i.e., ECoG. Usually, we use the montage illustrated in Fig. 2.1A. Six electrodes are located on the neocortex forming two anterior-posterior consecutive squares centered with respect to the midline, and the frontal square centered with respect to Bregma [all nearby neocortical electrodes are separated by the same distance, 5 mm, which is important for quantitative EEG (qEEG) analysis]. The electrodes are located bilaterally in primary motor cortex (M1: $L \pm 2.5$ mm, $AP + 2.5$ mm), primary

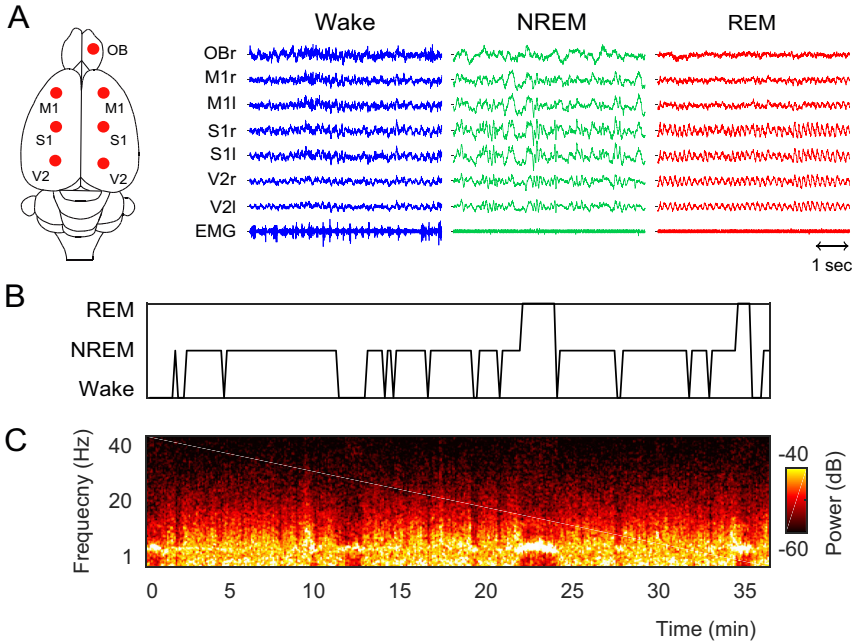

Figure 2.1 ***Polysomnographic recordings in the rat.*** (A) Schematic representation of the rat's brain along with the electrodes employed to record the intracranial electroencephalogram (referenced to the cerebellum). Representative traces are shown to the right of the panel for each one of the sleep-wake states. OB, olfactory bulb; M1, primary motor cortex; S1, primary somatosensory cortex; V2, secondary visual cortex; EMG, electromyogram; r and l, right and left hemispheres. (B) Hypnogram showing the sleep-wake states as a function of time. (C) Spectrogram showing the time-frequency representation of V2r cortex. *(Modified from Gonzalez, J., Cavelli, M., Mondino, A., Pascovich, C., Castro-Zaballa, S., Torterolo, P., Rubido, N., 2019. Decreased electrocortical temporal complexity distinguishes sleep from wakefulness. Sci. Rep. 9, 18457).*

somatosensory cortex (S1: L ± 2.5 mm, AP − 2.5 mm) and secondary visual cortex (V2: L ± 2.5 mm, AP − 7.5 mm, according to Paxinos and Watson atlas) (Paxinos and Watson, 2005). The other electrode is located over the right olfactory bulb (OB) (L: +1.25 mm, AP + 7.5 mm). A reference electrode is positioned above the cerebellum. To record the EMG, a pair of electrodes are inserted into the neck muscles. In rodents, the recordings of the ECoG and EMG are enough to identify W, NREM, and REM sleep states (there is no need to record the EOG). The electrodes are soldered into a 12-pin socket and fixed onto the skull with acrylic cement. After the animals recover from surgery, they are adapted to the recording chamber for 1 week.

The recordings are performed through a rotating connector to allow tethered rats to move freely within the recording box (freely movement condition). Bioelectric signals are amplified (×1000), filtered (0.1−500 Hz), sampled (1024 Hz, 16 bits), and stored in a PC using an acquisition software.

As in humans, to EOG, ECG and respiratory activity can be included in the recording. Also, deep electrodes may be added. For example, in cats, it is common to implant bipolar electrodes into the hippocampus to record theta oscillations, or into the lateral geniculate nucleus to record the ponto-geniculo-occipital (PGO) waves (Torterolo et al., 2016).

Another approach for recording is known as head-fixed or semi-restricted condition. In this case, the animal must be adapted to be in the recording position for several weeks. Wireless recordings, for example, by means of telemetry, have been developed since the late 70s (Neuhaus and Borbely, 1978). New technologies are increasing the possibilities for wireless PSG as well for others bioelectrical recordings (Fan et al., 2011).

Data analysis

In the rat, W and sleep are defined by PSG as follows (Fig. 2.1A): (1) W, by the presence of low voltage fast waves in frontal cortex, a mixed theta (4.5−9 Hz) activity in occipital cortex and relatively high EMG activity. (2) Light sleep, by the occurrence of high voltage slow cortical waves interrupted by low voltage fast EEG activity. (3) SWS, by the occurrence of continuous high amplitude slow (0.5−4 Hz) frontal and occipital waves and sleep spindles (similar to humans' spindles) combined with a reduced EMG activity; light sleep and SWS are grouped as NREM sleep. (4) REM sleep, by the presence of low voltage fast frontal waves, a regular theta rhythm in the occipital cortex (the origin of this rhythm is the hippocampus), and a silent EMG except for occasional myoclonic twitching.

A transitional state from SWS to REM sleep is often identified in the rat, and called intermediate state (IS) (Gottesmann, 1996). This state is a mixture of sleep spindles and theta activity. In the cat, this state is also signaled by the PGO waves that are better recorded from the lateral geniculate nucleus (Callaway et al., 1987). Single and large PGOs characterize the IS. At the onset of REM sleep, the frequency of the PGOs increases; they appear in bursts and decrease in amplitude. In the rat, only the "P" component of the PGO waves can be recorded from the pons (Datta and Hobson, 2000).

Total time spent in W, LS, SWS, NREM (NREM = LS + SWS), and REM sleep, as well as the duration and the number of episodes are determined. NREM and REM sleep latencies (from the beginning of the recording) is also included in the analysis. As is shown in Fig. 2.1B and C, the hypnogram associated to the spectrogram (that shows the power spectrum of the recorded ECoG signal, see below) is used to represent the W and sleep profile throughout the recording time.

Quantitative electroencephalogram analysis

qEEG is the field concerned with the numerical analysis of EEG or ECoG data, and associated behavioral correlates. These include linear and nonlinear analysis of the electrical activity that can be done either for human or animal recordings. Next, we will briefly comment on some prototypical ECoG analysis from rats that we perform in our laboratory.

Spectral power

The power spectral density of the EEG provides the weight of the frequency components of the signal. Mathematically, for a signal $x(t)$, its power spectral density is defined as

$$P_x(f) = |x(f)|^2$$

where

$$x(f) = \int_{-\infty}^{+\infty} x(t) e^{2\pi i f t} dt$$

is the Fourier transform of x. In practice, it is calculated by means of the Fast Fourier transform (FFT). The modern generic FFT algorithm was developed by Cooley and Tukey in 1965 (Coolye and Tukey, 1965), which increases the computation speed of the Fourier analysis simplifying its complexity. However, the FFT is seldom employed alone. In contrast, it is common to estimate the power spectral density by means of Welch's algorithm, which significantly reduces noise in the spectrum estimate. This method relies upon estimating the power spectrum in short time windows, employing the FFT, and then averaging the results to obtain a better estimate (which reduces the nonstationary components). It should be noted that these short windows are usually multiplied by a windowing function (i.e., Hamming, Hanning or Slepian functions) to reduce the distortion produced by the windows edges. The result is a representation of the

distribution of the energy or the amplitude of a signal in its different frequency components. The EEG power at a given frequency reflects the degree of local synchronization of the extracellular potential at that frequency (Buzsaki et al., 2012).

As it is shown in the spectrogram of Fig. 2.1C and in Fig. 2.2A, the analysis of the frequency content or power spectrum of the ECoG signal of the rat shows that in comparison with others behavioral states, the power of delta, theta, and sigma (sleep spindles) frequency bands during NREM sleep is high, while high frequency (>30 Hz) power values are low. During REM sleep, the power of high-frequency bands is intermediate between W and NREM sleep levels.

Another option to perform a spectral estimation is the wavelet transform (WT), in which any general function can be expressed as an infinite series of wavelets (Dhiman et al., 2013). Since WT allows the use of variable sized windows, it gives a more flexible time-frequency representation of a signal. To get a finer low-frequency resolution, long-time windows are used. In contrast, to get high-frequency information, short time windows are used.

Spectral coherence

Spectral coherence is a tool that is used to determine the degree of functional coupling between two cortical areas by means of the correlation between different frequency bands. In other words, it provides an objective

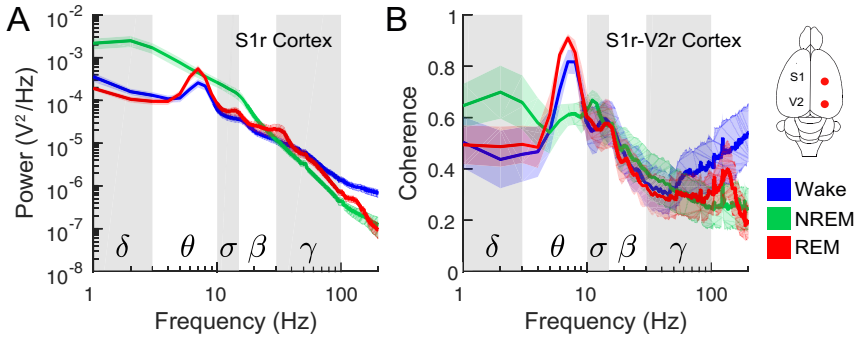

Figure 2.2 ***Power and coherence during wakefulness and sleep.*** (A) Power spectrum estimates from the right primary somatosensory cortex (S1r) during wakefulness, nonrapid eye movement and rapid eye movement sleep. Each trace shows the mean (solid line) +/− the standard error of the mean (shaded areas), $n = 6$. The frequency bands are shown with their corresponding Greek letters. (B) Coherence between S1r and right secondary visual cortex (V2r) during wakefulness, nonrapid eye movement and rapid eye movement sleep. Each trace shows the mean (solid line) +/− the standard error of the mean (shaded areas), $n = 6$.

index of functional interactions between different regions of the cerebral cortex. To be completely coherent, two waves must have a constant phase difference at a given frequency, and the relationship between the amplitudes at that frequency must be kept constant. This implies that two cortical areas that coordinate their electrical activity will present an increase in coherence between their electrical activities. It has therefore been proposed that the degree of coherence between the EEG of different cortices recorded simultaneously would reflect the strength of the functional interconnections (reentries) that occur between them (Bullock and McClune, 1989; Edelman and Tononi, 2000). The coherence is obtained from the cross spectral density (CSD, or the Fourier analysis of the cross-covariance function) between the two waves, normalized by the power of the spectral density of each wave. Therefore, the coherence between two waves *a* and *b*, at a given frequency *f*, is obtained as follows:

$$COH_{xy}(f) = \frac{\left|CSD_{xy}(f)\right|^2}{P_x(f)P_y(f)}$$

The coherence between two waveforms is a function of frequency and ranges from 0 for totally incoherent waveforms to 1 for maximal coherence. For two waveforms to be completely coherent at a particular frequency over a given time range, the phase shift between the waveforms must be constant and the amplitudes of the waves must have a constant ratio.

This function (magnitude-square cross coherence) evaluates both the amplitude and phase relationships. Importantly, the oscillations do not have to be fully synchronized to be consistent. These can be coupled between distant cortical areas with constant lag due to conduction and synaptic latencies, and still be coherent.

Fig. 2.2B shows an example where we analyze the intrahemispheric coherence between the right S1 and V2 channels across behavioral states. During W, there is a relatively large coherence in the theta band and in high-frequency components of the signal. On the contrary, during NREM sleep, coherence is high both in delta (slow oscillations) and sigma (spindle) bands. Interestingly, during REM sleep, there is a decrease in gamma coherence. High-gamma power (that reflect local synchronization) accompanied by minimal gamma coherence (that reflects long-range synchronization) is a trait that characterizes REM sleep, which is conserved in rodents, felines, and humans (Voss et al., 2009; Castro et al., 2013; Cavelli et al., 2015, 2017; Torterolo et al., 2016). A peak in what it is known as high-frequency oscillations (HFOs, about 120 Hz) is also observed (Cavelli et al., 2018).

Cross-frequency coupling

Apart from synchronization between areas at different frequency bands, the different frequency bands also interact within a single brain area in a phenomenon named cross-frequency coupling. This type of analysis thus allows to quantify whether fast oscillations (>30 Hz) "nest" in a certain phase of slower waves. One of the most studied forms of cross-frequency coupling is phase-amplitude coupling, which assesses whether the fast frequency envelope is modulated by the phase of a slower oscillation. This analysis is performed using the modulation index framework described by Tort (Tort et al., 2010). Briefly, the raw signal is filtered to obtain the slow frequency components, and then the phase time series is extracted from their analytical representation based on the Hilbert transform. In addition, the same raw signal is then also filtered to obtain the high-frequency components, and their amplitude time series are also obtained from their Hilbert analytical representation. Then, phase-amplitude distributions are computed between all slow-fast frequency combinations. Finally, the modulation index is obtained as $MI = (H\max - H)/H\max$, where $H\max$ is the maximum possible Shannon entropy for a given distribution [log(number of bins)], and H is the actual entropy of such distribution. For example, in Fig. 2.3, it is readily observed that the amplitude of high-frequency bands oscillations (120−160 Hz) is present in phase with the slow theta range oscillations (phase/amplitude coupling) during W and REM sleep (Cavelli et al., 2018; Gonzalez et al., 2020b). This is observable in both S1 and V2 cortex.

Complexity of the electrocorticogram signals

The complex nature of EEG or ECoG signals cannot be explained completely just by power and coherence analyses. In contrast, the field of nonlinear dynamics has developed measures and models that account for the complexity of the systems and their emerging interactions. A general approach to study time-signals is the characterization of their randomness or unpredictability of a signal.

One approach that has gained track over the last 20 years is the Ordinal Pattern (OP) analysis, which allows to encode any signal into OPs and approximate its Shannon entropy. The OPs are constructed by dividing a time-series $x(t)$ into nonoverlapping vectors (each of size D, commonly $D = 3,4$) and classifying each one according to the relative magnitude of its D elements. The classification is done by determining how many permutations are needed to order its elements increasingly; namely, an OP is

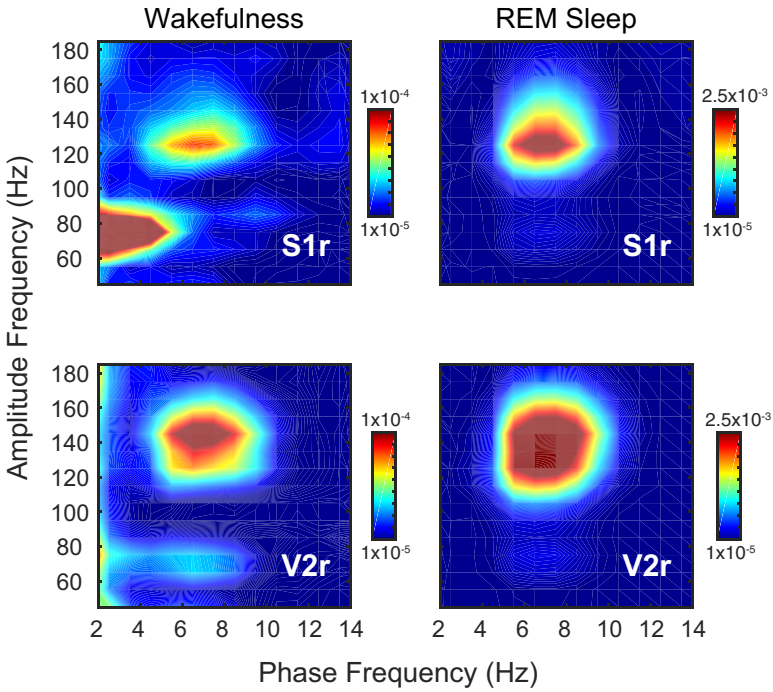

Figure 2.3 ***Phase amplitude coupling during wakefulness and rapid eye movement sleep.*** Comodulograms are shown for the S1r and V2r cortex. These plots indicate, through the color scale (modulation index), the amount of which the phase of the slow-frequency band (x-axis) modulates the amplitude of the high-frequency band (y-axis). Note that the modulation levels are one order of magnitude higher during rapid eye movement sleep (see the color calibration).

associated to represent the vector's permutations. For example, for $D = 2$, the time-series would be divided into vectors containing two consecutive values, such $\{x(t), x(t+1)\}$, These vectors have only two possible OPs for any time: either $x(t) > x(t+1)$ or $x(t) < x(t+1)$, which correspond to making 0 permutation or 1 permutation, respectively. It is worth noting that the number of possible permutations increases factorially with increasing vector length, i.e., for vectors of length D, there are $D!$ possible OPs. After that, the Shannon entropy

$$H(S) = -\sum_{x \in S} p(x) log[p(x)]$$

is computed from the OPs probability distribution, being S the alphabet containing each OP. This approximation is known as Permutation Entropy

(PeEn). In contrast to other methods, PeEn is a time-series complexity measure that is simple to implement, is robust to noise and short time-series, and works for arbitrary data sets. In particular, it has been shown that PeEn applied to EEG signals captures differences in waking and sleep states. Fig. 2.4 shows that the PeEN is larger during W and decreases during sleep (Gonzalez et al., 2019, 2020a). Importantly, the PeEn is highly dependent on the sampling frequencies employed, and can be therefore understood in terms of the ECoG's frequency content. Other metrics such as Lempel-Ziv are other options to evaluate the complexity of the signals.

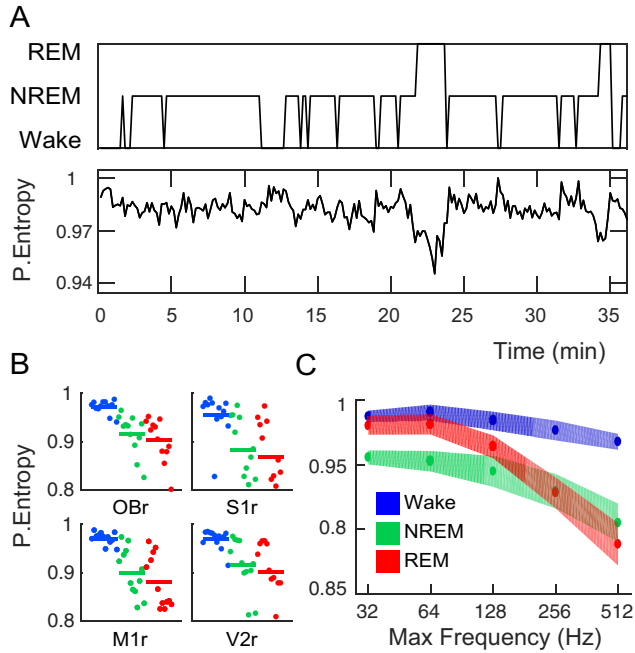

Figure 2.4 ***Temporal complexity during the sleep-wake states.*** (A) Top: Hypnogram showing the sleep-wake states as a function of time (same as in Fig. 2.1). Bottom: Temporal complexity as a function of time, estimated by Permutation Entropy. (B) PeEn values (for embedding dimension, $D = 3$) for 12 rats, differentiating each cortex electrode and sleep state (color code shown in panel C). Namely, each dot corresponds to the time-averaged PeEn value of each rat and cortex, where the horizontal bars are the population mean. (C) Average values of the seven cortical recording sites (shown in Fig. 2.1). Panel shows the averaged PeEn values as a function of the maximum frequency resolution (sampling frequency divided by 2, according to the Nyquist-Shannon criterion). Shaded areas in this panel depict the standard error of the mean for the PeEn, $n = 12$. *(Modified from Gonzalez, J., Cavelli, M., Mondino, A., Pascovich, C., Castro-Zaballa, S., Torterolo, P., Rubido, N., 2019. Decreased electrocortical temporal complexity distinguishes sleep from wakefulness. Sci. Rep. 9, 18457.)*

The entropy of a signal only gives information about the state of disorder of a single EEG channel. In our laboratory, we are also using a metric known as "mutual information" that assesses the amount of information shared between two cortical areas (Rubido et al., 2014; Bianco-Martinez et al., 2016; Garcia et al., 2020).

An important parameter to analyze is the sense of the information flow, i.e., "feedforward" (from primary to association cortex) versus "feedback" (from association to primary cortex), which has been seen to change across behavioral states. This could be done employing either "Granger Causality" or a time-lagged mutual information metric, such as Transfer Entropy (Imas et al., 2005). Both estimate the magnitude and direction of the temporal relationship between simultaneously recorded signals (Cekic et al., 2018) and are based on the statistical hypothesis that if A causes B, then the A's time series should be able to forecast or predict B.

Conclusion

In the present study, we have reviewed the main PSG procedures and data analysis for humans and animal models. Finally, we commented about important tools for the qEEG analysis that are widely used in research settings.

Acknowledgments

This study was supported by the "Programa de Desarrollo de las Ciencias Básicas, PEDECIBA" from Uruguay.

References

Andre, M., Lamblin, M.D., d'Allest, A.M., Curzi-Dascalova, L., Moussalli-Salefranque, F., T, S.N.T., Vecchierini-Blineau, M.F., Wallois, F., Walls-Esquivel, E., Plouin, P., 2010. Electroencephalography in premature and full-term infants. Developmental features and glossary. Neurophysiol. Clin. 40, 59–124.

Bianco-Martinez, E., Rubido, N., Antonopoulos Ch, G., Baptista, M.S., 2016. Successful network inference from time-series data using mutual information rate. Chaos 26, 043102.

Bullock, T.H., McClune, M.C., 1989. Lateral coherence of the electrocorticogram: a new measure of brain synchrony. Electroencephalogr. Clin. Neurophysiol. 73, 479–498.

Buzsaki, G., Anastassiou, C.A., Koch, C., 2012. The origin of extracellular fields and currents–EEG, ECoG, LFP and spikes. Nat. Rev. Neurosci. 13, 407–420.

Callaway, C.W., Lydic, R., Baghdoyan, H.A., Hobson, J.A., 1987. Pontogeniculooccipital waves: spontaneous visual system activity during rapid eye movement sleep. Cell. Mol. Neurobiol. 7, 105–149.

Carskadon, M.A., Dement, W., 2011. Normal human sleep: an overview. In: Kryger, M.H., Roth, T., Dement, W. (Eds.), Principles and Practices of Sleep Medicine. Elsevier-Saunders, Philadelphia, pp. 16–26.

Carskadon, M.A., Dement, W.C., 2017. Normal human sleep: an overview. In: Kryger, M.H., Roth, T., Dement, W.C. (Eds.), Principles and Practices of Sleep Medicine. Elsevier-Saunders, Philadelphia, pp. 15–24.

Castro, S., Falconi, A., Chase, M.H., Torterolo, P., 2013. Coherent neocortical 40-Hz oscillations are not present during REM sleep. Eur. J. Neurosci. 37, 1330–1339.

Cavelli, M., Castro, S., Schwarzkopf, N., Chase, M.H., Falconi, A., Torterolo, P., 2015. Coherent neocortical gamma oscillations decrease during REM sleep in the rat. Behav. Brain Res. 281, 318–325.

Cavelli, M., Castro-Zaballa, S., Mondino, A., Gonzalez, J., Falconi, A., Torterolo, P., 2017. Absence of EEG gamma coherence in a local activated neocortical state: a conserved trait of REM sleep. Trans. Brain Rhytmicity 2, 1–13.

Cavelli, M., Rojas-Libano, D., Schwarzkopf, N., Castro-Zaballa, S., Gonzalez, J., Mondino, A., Santana, N., Benedetto, L., Falconi, A., Torterolo, P., 2018. Power and coherence of cortical high-frequency oscillations during wakefulness and sleep. Eur. J. Neurosci. 48, 2728–2737.

Cekic, S., Grandjean, D., Renaud, O., 2018. Time, frequency, and time-varying Granger-causality measures in neuroscience. Stat. Med. 37, 1910–1931.

Coolye, J.W., Tukey, J.W., 1965. An algorithm for the machine calculation of complex Fourier series. Math. Comput. 19, 297–301.

Datta, S., Hobson, J.A., 2000. The rat as an experimental model for sleep neurophysiology. Behav. Neurosci. 114, 1239–1244.

Dhiman, R., Priyanka, Saini, J.S., 2013. Wavelet analysis of electrical signals from brain: the electroencephalogram. In: Singh, H., Awasthi, A.K., Mishra, R. (Eds.), Quality, Reliability, Security and Robustness in Heterogeneous Networks, pp. 283–289.

Edelman, G.M., Tononi, G., 2000. A Universe of Consciousness. Basic Books, New York.

Fan, D., Rich, D., Holtzman, T., Ruther, P., Dalley, J.W., Lopez, A., Rossi, M.A., Barter, J.W., Salas-Meza, D., Herwik, S., Holzhammer, T., Morizio, J., Yin, H.H., 2011. A wireless multi-channel recording system for freely behaving mice and rats. PLoS One 6, e22033.

Garcia, R.A., Marti, A.C., Cabeza, C., Rubido, N., 2020. Small-worldness favours network inference in synthetic neural networks. Sci. Rep. 10, 2296.

Gergely, A., Kiss, O., Reicher, V., Iotchev, I., Kovacs, E., Gombos, F., Benczur, A., Galambos, A., Topal, J., Kis, A., 2020. Reliability of family dogs' sleep structure scoring based on manual and automated sleep stage identification. Animals (Basel) 10.

Gonzalez, J., Cavelli, M., Mondino, A., Pascovich, C., Castro-Zaballa, S., Rubido, N., Torterolo, P., 2020a. Electrocortical temporal complexity during wakefulness and sleep: an updated account. Sleep Sci. 47–50.

Gonzalez, J., Cavelli, M., Mondino, A., Pascovich, C., Castro-Zaballa, S., Torterolo, P., Rubido, N., 2019. Decreased electrocortical temporal complexity distinguishes sleep from wakefulness. Sci. Rep. 9, 18457.

Gonzalez, J., Cavelli, M., Mondino, A., Rubido, N., Bl Tort, A., Torterolo, P., 2020b. Communication through coherence by means of cross-frequency coupling. Neuroscience 449, 157–164.

Gordon, R., Rzempoluck, E.J., 2004. Introduction to laplacian montages. Am. J. Electroneurodiagn. Technol. 44, 98–102.

Gottesmann, C., 1996. The transition from slow-wave sleep to paradoxical sleep: evolving facts and concepts of the neurophysiological processes underlying the intermediate stage of sleep. Neurosci. Biobehav. Rev. 20, 367–387.

Graven, S., 2006. Sleep and brain development. Clin. Perinatol. 33, 693–706 (vii).

Grigg-Damberger, M.M., 2016. The visual scoring of sleep in infants 0 to 2 Months of age. J. Clin. Sleep Med. 12, 429–445.

Imas, O.A., Ropella, K.M., Ward, B.D., Wood, J.D., Hudetz, A.G., 2005. Volatile anesthetics disrupt frontal-posterior recurrent information transfer at gamma frequencies in rat. Neurosci. Lett. 387, 145–150.

Keenan, S., Hirshkowitz, M., 2017. Sleep stage scoring. In: Kryger, M.H., Roth, T., Dement, W.C. (Eds.), Principles and Practices of Sleep Medicine. Elsevier-Saunders, Philadelphia, pp. 1567–1575.

Kis, A., Szakadat, S., Kovacs, E., Gacsi, M., Simor, P., Gombos, F., Topal, J., Miklosi, A., Bodizs, R., 2014. Development of a non-invasive polysomnography technique for dogs (*Canis familiaris*). Physiol. Behav. 130, 149–156.

Lachaux, J.P., Rudrauf, D., Kahane, P., 2003. Intracranial EEG and human brain mapping. J. Physiol. Paris 97, 613–628.

Lopes da Silva, F., 2010. EEG: origin and measurement. In: Mulert, C., Lemieuz, L. (Eds.), EEG-fMRI. Springer-Verlag, Berlin, pp. 19–38.

Markwald, R.R., Bessman, S.C., Reini, S.A., Drummond, S.P., 2016. Performance of a portable sleep monitoring device in individuals with high versus low sleep efficiency. J. Clin. Sleep Med. 12, 95–103.

Mirmiran, M., Maas, Y.G., Ariagno, R.L., 2003. Development of fetal and neonatal sleep and circadian rhythms. Sleep Med. Rev. 7, 321–334.

Neuhaus, H.U., Borbely, A.A., 1978. Sleep telemetry in the rat. II. Automatic identification and recording of vigilance states. Electroencephalogr. Clin. Neurophysiol. 44, 115–119.

Paxinos, G., Watson, C., 2005. The Rat Brain. Academic Press, New York.

Rubido, N., Martí, A.C., Bianco-Martínez, E., Grebogi, C., Baptista, M.S., Masoller, C., 2014. Exact detection of direct links in networks of interacting dynamical units. New J. Phys. 16, 093010.

Tort, A.B., Komorowski, R., Eichenbaum, H., Kopell, N., 2010. Measuring phase-amplitude coupling between neuronal oscillations of different frequencies. J. Neurophysiol. 104, 1195–1210.

Torterolo, P., Castro-Zaballa, S., Cavelli, M., Chase, M.H., Falconi, A., 2016. Neocortical 40 Hz oscillations during carbachol-induced rapid eye movement sleep and cataplexy. Eur. J. Neurosci. 43, 580–589.

Torterolo, P., Castro-Zaballa, S., Cavelli, M., Gonzalez, J., 2019. Arousal and normal conscious cognition. In: Garcia-Rill, E. (Ed.), Arousal in Neurological and Psychiatric Diseases, pp. 1–24.

Voss, U., Holzmann, R., Tuin, I., Hobson, J.A., 2009. Lucid dreaming: a state of consciousness with features of both waking and non-lucid dreaming. Sleep 32, 1191–1200.

Wohr, A., Kalus, M., Reese, S., Fuchs, C.S., Erhard, M., 2016. Equine sleep behaviour and physiology based on polysomnographic examinations. Equine Vet. J. 48, 9.

Zheng, G., Qi, X., Li, Y., Zhang, W., Yu, Y., 2018. A comparative study of standardized infinity reference and average reference for EEG of three typical brain states. Front. Neurosci. 12, 158.